

# Total emission control for glass melting furnace using plasma PM conversion process

Tomoyuki Kuroki<sup>1,\*</sup>, Taiga Tanaka<sup>1</sup>, Haruhiko Yamasaki<sup>1</sup>,  
Hashira Yamamoto<sup>2</sup>, Masaaki Okubo<sup>1</sup>

<sup>1</sup> Department of Mechanical Engineering, Osaka Metropolitan University, Japan

<sup>2</sup> Environmental Affairs Office, Nihon Yamamura Glass Co., Ltd., Japan

\* Corresponding author: [kuroki@omu.ac.jp](mailto:kuroki@omu.ac.jp) (Tomoyuki Kuroki)

Received: 30 December 2024

Revised: 14 February 2025

Accepted: 28 February 2025

Published online: 10 March 2025

## Abstract

In glass bottle manufacturing plants, products are formed by melting raw materials at approximately 1500 °C using heavy oil and liquefied natural gas (LNG) in a melting furnace. The exhaust gas generated during this process contains nitrogen oxides (NO<sub>x</sub>), sulfur oxides (SO<sub>x</sub>), and particulate matter (PM), which contribute to environmental contamination when released into the atmosphere. Conventional exhaust treatment systems for glass melting furnaces typically include wet or semi-dry desulfurization equipment utilizing sodium hydroxide (NaOH), a compound that readily reacts with sulfur dioxide (SO<sub>2</sub>), and dust collectors such as electrostatic precipitators or bag filters that primarily collect sodium sulfite (Na<sub>2</sub>SO<sub>3</sub>) and sodium sulfate (Na<sub>2</sub>SO<sub>4</sub>) produced during the desulfurization process, effectively enabling desulfurization and PM removal. However, they lack an efficient method for NO<sub>x</sub> removal due to the presence of catalyst poisons, including sticky dust, in the exhaust gas. This study proposes a plasma-chemical hybrid process (PCHP) for the simultaneous removal of NO<sub>x</sub> and SO<sub>x</sub>. This process integrates plasma oxidation with chemical reduction and can be incorporated into existing desulfurization reactors. Furthermore, this study applies PCHP to an operational glass melting furnace exhaust gas treatment system, achieving simultaneous removal of PM, NO<sub>x</sub>, and SO<sub>2</sub>.

**Keywords:** Plasma-chemical hybrid process, denitration, desulfurization, glass melting furnace.

## 1. Introduction

In glass manufacturing plants, significant amounts of fossil fuels, such as heavy oil and liquefied natural gas (LNG), are consumed in furnaces to melt glass raw materials at high temperatures of approximately 1500°C. This process generates large volumes of exhaust gas containing nitrogen oxides (NO<sub>x</sub>), sulfur oxides (SO<sub>x</sub>), carbon dioxide (CO<sub>2</sub>), carbon monoxide (CO), and particulate matter (PM). Among these, NO<sub>x</sub>, SO<sub>x</sub>, and PM are pollutants that must be reduced before being released into the atmosphere. Fig. 1 illustrates a typical exhaust gas treatment process used in glass manufacturing plants. Sulfur dioxide (SO<sub>2</sub>) is initially treated with an aqueous solution of sodium hydroxide (NaOH) in semi-dry or wet desulfurization equipment, as SO<sub>2</sub> readily reacts with alkaline solutions such as NaOH [1]. Sodium sulfite (Na<sub>2</sub>SO<sub>3</sub>) and sodium sulfate (Na<sub>2</sub>SO<sub>4</sub>) produced during the desulfurization process are collected using dust collectors, such as electrostatic precipitators (ESPs) and bag filters. The collected Na<sub>2</sub>SO<sub>4</sub> particles are then reused as raw materials for glass production. In contrast, equipment for NO<sub>x</sub> removal is not typically installed. Although selective catalytic reduction (SCR) [2] is widely used in thermal power plants and waste disposal facilities to remove NO<sub>x</sub>, its application to glass melting furnaces is challenging. Exhaust gases from these furnaces contain alkali metals and sulfur compounds, which poison the catalyst and reduce SCR performance [3–5]. Consequently, NO<sub>x</sub> suppression in glass melting furnaces is primarily achieved through the use of low-NO<sub>x</sub> burners [6] and low air-fuel ratio combustion. However, these methods achieve only limited reductions in NO<sub>x</sub> emissions [7]. Moreover, low air-fuel ratio combustion can lead to issues such as fuel loss due to incomplete combustion. Given these challenges, there is a strong demand for effective denitration technology that can be applied to the exhaust gases from glass melting furnaces.

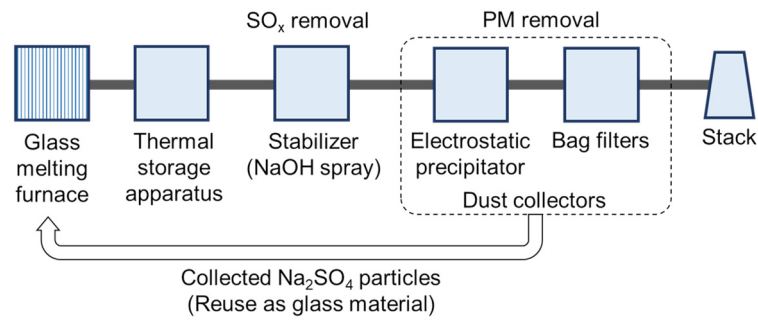


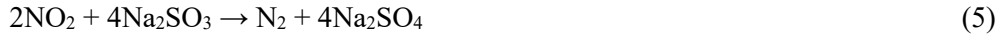
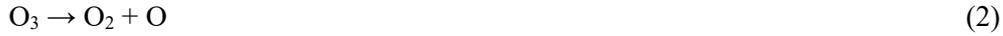
**Fig. 1.** Typical exhaust gas treatment flow conducted in glass manufacturing plants.

The plasma-chemical hybrid process (PCHP) is a relatively new exhaust gas purification technology that combines plasma and chemical processes. This system is anticipated to be highly efficient and energy-saving, contributing to global environmental protection by eliminating  $\text{NO}_x$  emissions from various sources, including boilers, marine diesel engines, industrial incinerators, diesel generators [8–18], and semiconductor manufacturing exhaust gases [19]. In the PCHP, the plasma component oxidizes nitrogen monoxide ( $\text{NO}$ ), the primary constituent of  $\text{NO}_x$  in exhaust gases and poorly soluble in water, into nitrogen dioxide ( $\text{NO}_2$ ) using ozone ( $\text{O}_3$ ) generated by nonthermal plasma. The generated  $\text{NO}_2$  is then chemically reduced using a  $\text{Na}_2\text{SO}_3$  solution. Simultaneously, flue gases containing  $\text{SO}_2$  are treated with a  $\text{NaOH}$  solution in wet or semi-dry desulfurization units, as  $\text{SO}_2$  readily reacts with alkaline solutions [20], producing  $\text{Na}_2\text{SO}_3$ . This  $\text{Na}_2\text{SO}_3$  solution is used to reduce  $\text{NO}_2$ , generating products that are subsequently dried and collected as PM, such as  $\text{Na}_2\text{SO}_4$ , through downstream ESPs and bag filters. In the glass industry, the collected  $\text{Na}_2\text{SO}_4$  can be recycled as raw material, enhancing the suitability of PCHP as an aftertreatment technology for glass melting furnaces. Additionally, PCHP facilitates complete combustion by enabling a higher air ratio, reducing fuel consumption and associated costs, and mitigating  $\text{CO}_2$  emissions. Its retrofit capability allows integration with existing wet and semi-dry desulfurization plants, reducing both installation costs and energy consumption. The high efficiency of the PCHP for  $\text{NO}_2$  removal was previously demonstrated through small-scale laboratory experiments [21–23]. Additionally, a small-scale simulation model for  $\text{NO}$  oxidation by  $\text{O}_3$  in a two-phase flow was successfully developed [24]. Building on these findings, PCHP was integrated into the desulfurization system of an operational glass melting furnace for practical demonstration and evaluation [25–28]. Pilot-scale experiments revealed that achieving high desulfurization and denitrification efficiency with PCHP required the flow rate of the  $\text{NaOH}$  solution to be double that of the cooling water used to envelope the  $\text{O}_3$  [27]. This increased flow rate was necessary because  $\text{SO}_2$  is more prevalent than  $\text{NO}$  in exhaust gases, and  $\text{SO}_2$  reduction by  $\text{NaOH}$  enhances the formation of  $\text{SO}_3^{2-}$ , improving  $\text{NO}_x$  removal efficiency. In this study, the  $\text{NaOH}$  solution injection rate was further increased, and  $\text{Na}_2\text{SO}_3$  was added to the  $\text{NaOH}$  solution to enhance  $\text{NO}_x$  removal. Additionally, the angle of the  $\text{NaOH}$  spray nozzle was adjusted to optimize desulfurization with reduced  $\text{NaOH}$  usage, and the solution injection zone was expanded. The performances of simultaneous desulfurization and denitrification were also evaluated.

## 2. Chemical reactions in denitration and desulfurization by PCHP

The semi-dry PCHP combines a plasma-based process, utilizing air-reactive gases generated from a nonthermal plasma reactor (primarily ozone,  $\text{O}_3$ ), with a chemical process that employs  $\text{NaOH}$  as a reducing agent and neutralizer for the removal of  $\text{NO}_x$  and  $\text{SO}_2$ . In the plasma process,  $\text{NO}$  in the exhaust gas is oxidized by  $\text{O}_3$ , generated from the nonthermal plasma reactor using oxygen gas as the raw material, into water-soluble  $\text{NO}_2$  via reaction (1). Since  $\text{O}_3$  thermally decomposes at temperatures exceeding  $150^\circ\text{C}$ , cooling water is simultaneously sprayed with  $\text{O}_3$  using a two-phase flow nozzle. This creates a localized cooling zone where the temperature drops below  $150^\circ\text{C}$ , facilitating the oxidation of  $\text{NO}$  by  $\text{O}_3$ . Some  $\text{O}_3$  molecules decompose into oxygen radicals ( $\text{O}\cdot$ ) through reaction (2), and these radicals further oxidize  $\text{NO}$  via reaction (3). In glass melting furnaces,  $\text{SO}_2$ , generated from fuel and raw materials, is neutralized by spraying an aqueous  $\text{NaOH}$  solution, as shown in reaction (4). This reaction produces  $\text{Na}_2\text{SO}_3$ , a compound with strong reducing properties. The  $\text{Na}_2\text{SO}_3$  facilitates the liquid-phase reduction of  $\text{NO}_2$  to  $\text{N}_2$ , while itself being oxidized to  $\text{Na}_2\text{SO}_4$  via reaction (5). In its semi-dry state,  $\text{Na}_2\text{SO}_4$  is completely dried by the heat of the exhaust gas. The  $\text{Na}_2\text{SO}_4$

particles are then collected using an electrostatic precipitator and bag filter. These particles are subsequently reused as raw materials in the glass manufacturing process, enhancing the sustainability of the system.



### 3. Experimental setup and methods

#### 3.1 Plasma ozonizer

Two pilot-scale plasma ozonizers (SAGT4M-C and SAGT6M-C; Sumitomo Precision Products Co., Ltd.) are operated in parallel to generate  $\text{O}_3$  at a combined rate of  $10 \text{ kg h}^{-1}$ , scalable to industrial equipment. Detailed specifications of the plasma ozonizers are provided in Table 1. Each ozonizer comprises nonthermal plasma reactors and is supplied with 99.5%  $\text{O}_2$  gas from a cold evaporator tank containing liquid  $\text{O}_2$ . Flow rates of  $26.7 \text{ Nm}^3 \text{ h}^{-1}$  and  $40.0 \text{ Nm}^3 \text{ h}^{-1}$  are introduced into the SAGT6M-C and SAGT4M-C ozonizers, respectively. The ozone mass flow rate is adjustable by varying the output of the high-voltage power supply unit, with capacities ranging from 0 to 6 kg/h for the SAGT6M-C and 0 to 4 kg/h for the SAGT4M-C. The  $\text{O}_3$  concentration is monitored using ultraviolet absorption ozone monitors (EG-600; 0–200  $\text{g Nm}^{-3}$ ; Ebara Jitsugyo Co., Ltd.). The SAGT6M-C and SAGT4M-C models contain 432 and 334 glass plasma reactors, respectively, each cooled with water at  $15^\circ\text{C}$  to ensure consistent ozone output during extended operation. Plasma is generated within the glass reactors via dielectric barrier discharge between the glass and water-cooled ground electrodes (Fig. 2). To maintain operational symmetry, the glass plasma reactors, each approximately 1400 mm in length, are installed with careful alignment.

**Table 1.** Specifications of plasma ozonizers.

Model	Sumitomo Precision Products Co., Ltd.	
	SAGT4M-C	SAGT6M-C
Plasma generation type	Dielectric barrier discharge with water-cooled electrodes	
Number of glass plasma reactors	334	432
Discharge voltage	5 kV	
Maximum ozone generation rate	$4.0 \text{ kg h}^{-1}$	$6.0 \text{ kg h}^{-1}$
Ozone concentration	$150 \text{ g}/(\text{Nm}^3 \text{ h}^{-3}) (= 7.0\%)$	
Oxygen pressure at the inlet	0.13 MPa	
Oxygen flow rate at the inlet	$26.7 \text{ Nm}^3 \text{ h}^{-1}$	$40.0 \text{ Nm}^3 \text{ h}^{-1}$
Oxygen pressure at the outlet	$\sim 0.12 \text{ MPa}$	
Flow rate of cooling water	$102 \text{ L min}^{-1}$	$153 \text{ L min}^{-1}$
Cooling water temperature	$15^\circ\text{C}$ at the inlet (temperature difference is approximately $5^\circ\text{C}$ )	
Width of ozone generation control	10%–100% of the maximum generation	
Power consumption	28 kW	48 kW
Power source	AC 400 V, three-phase, 50 Hz	

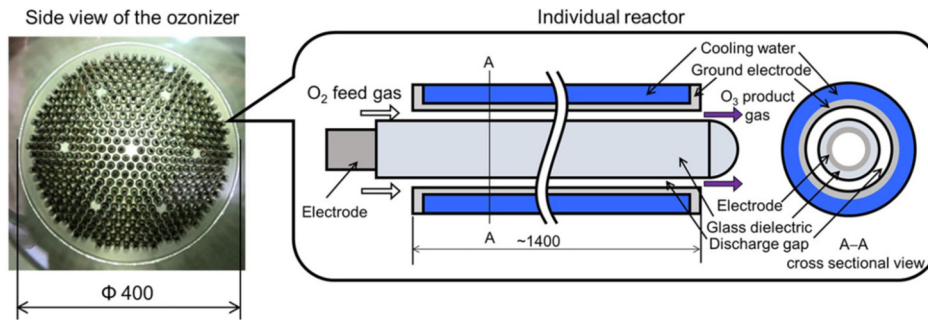


Fig. 2. Glass plasma reactor generates plasma through the dielectric barrier discharge between the glass and water-cooled ground electrodes [28].

### 3.2 Experimental setup and methods

Experiments were conducted using a semi-dry exhaust gas aftertreatment system installed on a glass furnace at the Nihon Yamamura Glass Tokyo Plant. Glass furnace operations involve heating raw materials to approximately 1500 °C using fossil fuels such as C-heavy oil and LNG. Achieving such high temperatures solely through LNG combustion is technically infeasible; thus, C-heavy oil is added, comprising 25–33% of the total fuel. An electric heater is also used to preheat the raw materials. The furnace's total thermal input, including contributions from C-heavy oil, LNG, and the electric heater, is approximately 10 MW. The volume of combustion air is regulated using the air ratio, which ensures compliance with NO<sub>x</sub> emission regulations. The air ratio is defined as the ratio between the theoretical air volume required for complete combustion of the heavy oil and LNG mixture and the actual input combustion air volume, adjusted for the combustion percentage of the heavy oil. To reduce NO<sub>x</sub> emissions, fossil fuel usage must be increased, and air ratios must be decreased.

The reactor is a cylindrical apparatus ( $\phi 3.5 \times \sim 15$  m, Asahi Glass Engineering Co., Ltd.) equipped with three-fluid spray nozzles for O<sub>3</sub> gas cooling and two-fluid spray nozzles for desulfurization (Fig. 3). The detailed arrangement of the nozzles is illustrated in Fig. 4. By operating two plasma ozonizers in parallel, ozone is injected into the semi-dry reactor at a rate of approximately 10 kg h<sup>-1</sup>.

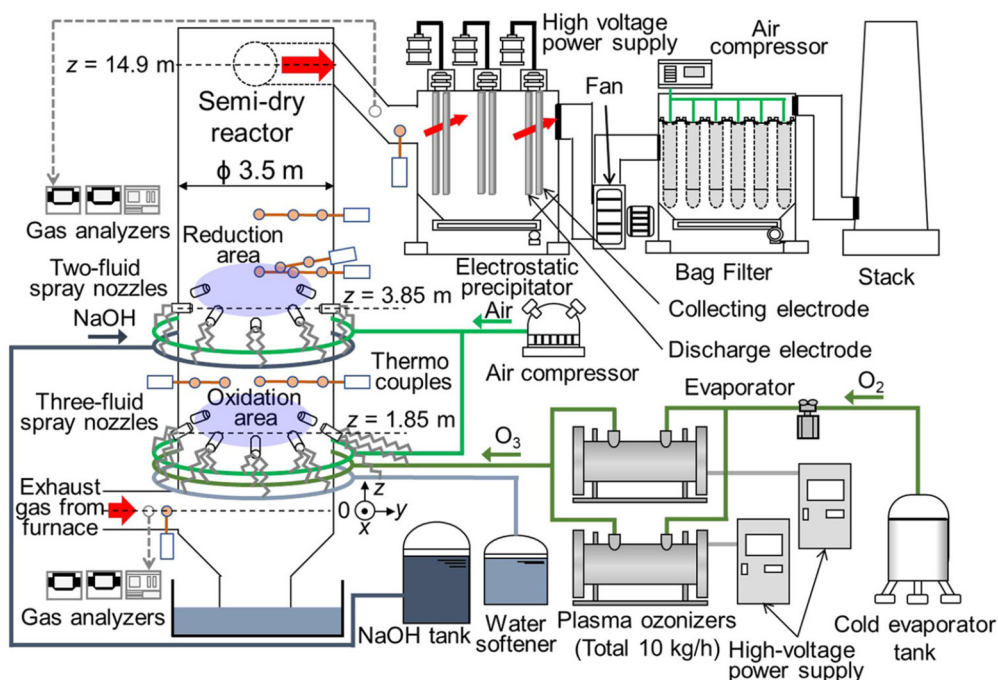


Fig. 3. Schematic diagram of the semi-dry aftertreatment system with the plasma-chemical hybrid process in the glass melting furnace [28].

Ozone is introduced into the flue gas along with cooling water and compressed air through a three-fluid nozzle positioned at a height ( $z$ ) of 1.85 m in the reactor.  $\text{NO}_2$ , generated in the oxidation region, is subsequently reduced to  $\text{N}_2$  by reactive species formed from the interaction of  $\text{NaOH}$  and  $\text{SO}_2$ . These reactive species are injected through a two-fluid nozzle located horizontally at  $z = 3.85$  m downstream of the reactor inlet. Simultaneously, a solution containing  $\text{SO}_4^{2-}$  is formed, which dries near the reactor outlet to produce  $\text{Na}_2\text{SO}_4$  dust particles. These particles are collected downstream using dust collectors comprising a dry ESP and bag filters. The pressure drop across the two spraying regions is approximately 8 Pa.

To evaluate the  $\text{NO}_x$  and  $\text{SO}_x$  aftertreatment performance of the semi-dry PCHP, the concentrations of exhaust gas components were measured at both the reactor inlet and outlet.  $\text{NO}_x$  and  $\text{SO}_x$  concentrations were converted to equivalent values using the following equation:

$$A = \frac{21-15}{21-C} B \quad (6)$$

where  $A$  represents the converted  $\text{NO}_x$  or  $\text{SO}_x$  concentration based on  $[\text{O}_2] = 15\%$ ,  $B$  is the measured  $\text{NO}_x$  or  $\text{SO}_x$  concentration, and  $C$  is the measured  $\text{O}_2$  concentration. The removal efficiencies of  $\text{NO}$ ,  $\text{SO}_2$ , and  $\text{NO}_x$  are calculated using their molar flow rates. To confirm the formation of the localized cooling region, exhaust gas temperatures were measured at the reactor inlet, outlet, and at four downstream heights inside the reactor ( $z = 0, 2.85, 4.35, \text{ and } 5.85$  m). Five measurements were taken at  $z = 2.85$  m and  $z = 4.35$  m, and three measurements were taken at  $z = 5.85$  m.  $\text{SO}_2$  analyzers (IRA-208, Shimadzu Corporation; VA-3000, PG-337, and PG-350, Horiba Ltd.),  $\text{NO}$  analyzers (PG-240, PG-337, PG-340, and PG-350, Horiba Ltd.), and  $\text{NO}_x$  analyzers (NOA7000, NOA7100, and IRA-208, Shimadzu Corporation) were used to assess gas levels.

Table 2 lists the experimental conditions of experiments conducted in August 2020 and October 2020, which investigated variations in parameters such as the flow rates of  $\text{O}_3$  gas, water spray,  $\text{NaOH}$  solution spray, and  $\text{NaOH}$  concentration. In the August 2020 experiment, the water and solution spray flow rates were slightly reduced during the T9–T11 periods because the exhaust gas temperature at the reactor outlet was about to drop below the reference value for operation in the T8 period. The nozzle tips were installed at a  $30^\circ$  upward angle in a vertical direction, with a spray angle of  $20^\circ$ . During the October 2020 experiment, the nozzle tips alternated between horizontal and vertical directions at  $30^\circ$  upward, depending on the nozzle position, with spray angles of  $20^\circ$  and  $60^\circ$ . Two- and three-fluid nozzles were installed at the same position in the cross-sectional direction ( $x$ - $y$  plane) but  $40^\circ$  apart in the circumferential direction (Fig. 4). Compressed air (0.2 MPa) and soft water ( $0.20$ – $0.52 \text{ m}^3 \text{ h}^{-1}$ , 0.2 MPa) were sprayed using a three-fluid nozzle to form water mists with  $50 \mu\text{m}$  droplets. Similarly, a two-fluid nozzle was used to spray compressed air (0.2 MPa) and  $\text{NaOH}$  solution ( $0$ – $0.93 \text{ m}^3 \text{ h}^{-1}$ , 0.2 MPa) to form  $\text{NaOH}$  solution mists with  $40 \mu\text{m}$  droplets (Sauter mean diameter).

**Table 2.** Experimental conditions.

Test periods	Exhaust gas flow rate (dry base) $\text{Nm}^3 \text{ h}^{-1}$	$\text{O}_3$ injection		$\text{NaOH}$ solution spray			$\text{O}_3$ spray nozzles ( $z = 1.85$ mm)	$\text{NaOH}$ solution spray nozzles ( $z = 3.85$ mm)
		Injected $\text{O}_3$ $\text{kg h}^{-1}$	Water spray $\text{m}^3 \text{ h}^{-1}$	$\text{NaOH}$ %	$\text{Na}_2\text{SO}_3$ %	Solution spray $\text{m}^3 \text{ h}^{-1}$		
T4	13250	0	0.52	4.0	0	0.51		
T5	13250	10.8	0.52	4.0	0	0.51		
T6	13100	0	0.52	4.3	1.0	0.51		
T7	13100	10.9	0.52	4.3	1.0	0.51		
T8	13300	0	0.23	2.2	0	0.93		A
T9	13300	10.6	0.20	2.2	0	0.91	A	
T10	13250	0	0.20	2.5	1.0	0.91		
T11	13250	10.6	0.20	2.5	1.0	0.91		
T4	14050	10.6	0.41	4.0	0	0.49		
T5	14050	10.7	0.41	4.0	0	0.48		Nos.1,3,5,7: A
T6	14050	10.7	0.41	4.0	0	0.48		Nos.2,4,6: B

## 4. Results and discussion

Fig. 5 shows the time-dependent NO concentrations at the reactor inlet and outlet during the T4–T7 period (August 2020). The NO concentrations are converted based on an oxygen concentration of 15%. The average NO concentrations at the reactor inlet and outlet during the T4, T5, T6, and T7 periods are 215, 214, 212, and 213 ppm, and 222, 136, 217, and 132 ppm, respectively. During the T4 and T6 periods, the NO concentrations at both the inlet and outlet are nearly the same, indicating that NO oxidation does not occur due to factors such as O<sub>2</sub> availability.

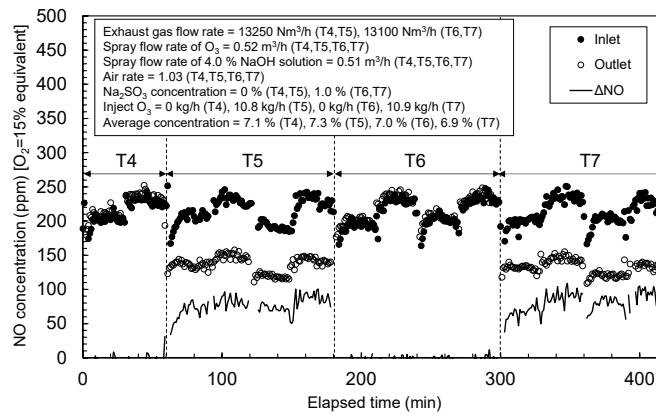


**Fig. 5.** Time-dependent NO concentrations at the reactor inlet and outlet in the T4–T7 test periods (August 2020).

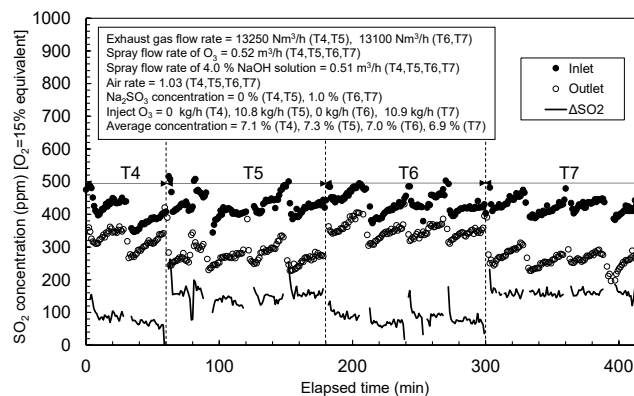


**Fig. 6.** Time-dependent SO<sub>2</sub> concentrations at the reactor inlet and outlet in the T4–T7 test periods (August 2020).

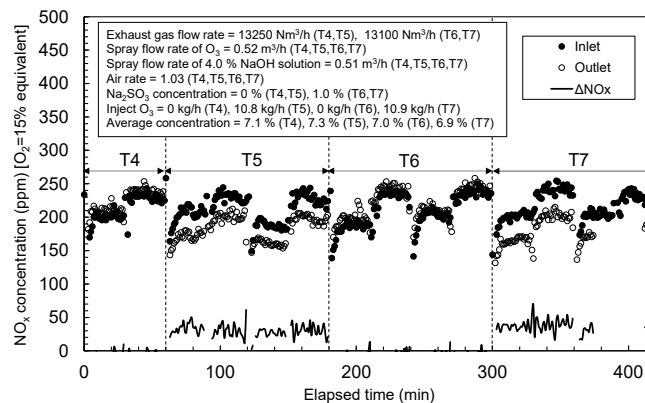
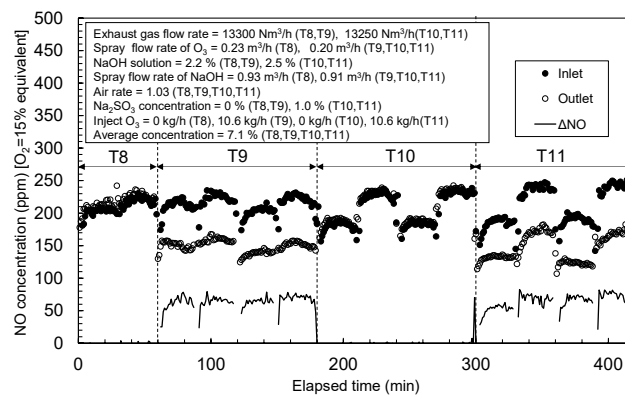


**Fig. 7.** Time-dependent NO<sub>x</sub> concentrations at the reactor inlet and outlet in the T4–T7 test periods (August 2020).

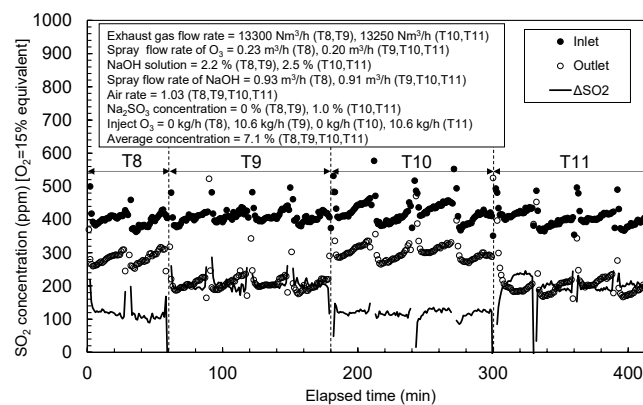
During the T5 and T7 periods, NO at the reactor outlet is oxidized to NO<sub>2</sub>, and the NO concentration decreases upon the injection of O<sub>3</sub> into the localized cooling zone formed by the three-fluid nozzles. The amount of ozone generated by the ozonizers is insufficient for the amount of NO contained in the exhaust gas. Therefore, the molar ratios of the injected O<sub>3</sub> to NO in the exhaust gas during the T5 and T7 periods are 0.75 and 0.73, respectively. The ratios of the difference in molar flow rates of NO at the reactor inlet and outlet to the molar flow rate of the injected O<sub>3</sub> ( $\Delta\text{NO}/\text{O}_3$ ) during the T5 and T7 periods are 0.43 and 0.46, respectively, with NO removal efficiencies of 32 and 33%, respectively. Ozone thermally decomposes at high temperatures (> 150 °C), as shown in reaction (2). Some of the O radicals produced by this thermal decomposition facilitate the oxidation of NO via reaction (3), while the remaining O radicals react with O<sub>3</sub> to form oxygen, as expressed in reaction (7).



Fig. 6 shows the time-dependent SO<sub>2</sub> concentrations at the reactor inlet and outlet during the T4–T7 periods (August 2020). The average SO<sub>2</sub> concentrations at the reactor inlet and outlet during the T4, T5, T6, and T7 periods are 407, 428, 436, and 425 ppm, and 323, 274, 350, and 264 ppm, respectively. SO<sub>2</sub> removal efficiencies of 19, 32, 13, and 33% are achieved in the T4, T5, T6, and T7 periods, respectively. These results indicate that the injection of ozone into the reactor enhances desulfurization. Ozone is believed to convert SO<sub>2</sub> into SO<sub>3</sub>, which activates the absorption reaction in the NaOH solution. The NaOH solution in T6 and T7 contains 1.0% Na<sub>2</sub>SO<sub>3</sub>; however, no effect of Na<sub>2</sub>SO<sub>3</sub> on desulfurization is observed.



**Fig. 8.** Time-dependent NO concentrations at the reactor inlet and outlet in the T8–T11 test periods (August 2020).



**Fig. 9.** Time-dependent SO<sub>2</sub> concentrations at the reactor inlet and outlet in the T8–T11 test periods (August 2020).

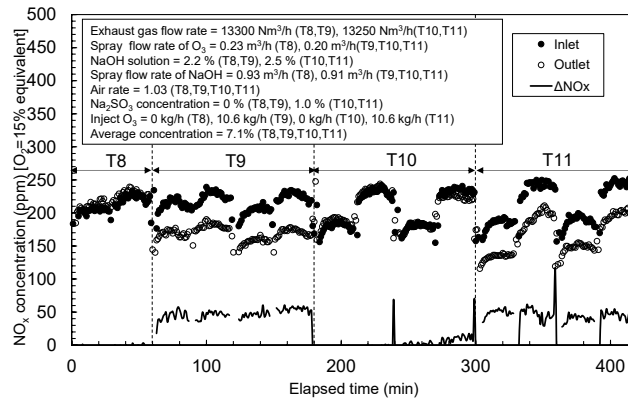


**Fig. 10.** Time-dependent  $\text{NO}_x$  concentrations at the reactor inlet and outlet in the T8–T11 test periods (August 2020).

Oxidized  $\text{NO}_2$  is reduced to  $\text{N}_2$  by the  $\text{SO}_3^{2-}$  ion, as depicted in reaction (5), which is a byproduct of desulfurization in the localized cooling zone. Fig. 7 shows the time-dependent  $\text{NO}_x$  concentrations at the reactor inlet and outlet during the T4–T7 periods (August 2020). The average  $\text{NO}_x$  concentrations at the reactor inlet and outlet during the T4, T5, T6, and T7 periods are 214, 212, 211, and 217 ppm, and 224, 182, 221, and 178 ppm, respectively. The  $\text{NO}_x$  concentrations at the reactor inlet and outlet during the T4 and T6 periods are similar. The  $\text{NO}_x$  component is primarily  $\text{NO}$  because its concentration of  $\text{NO}_x$  remains unchanged, implying that the denitration effect is not achieved.  $\text{NO}$  is oxidized to  $\text{NO}_2$  during the T5 and T7 periods, resulting in a lower concentration of  $\text{NO}$ . The concentration of  $\text{NO}$  also decreases due to the injection of  $\text{O}_3$  into the localized cooling zone and the  $\text{NaOH}$  solution spray.  $\text{NO}_x$  removal efficiencies of 0%, 8.3%, 0%, and 12% are observed in the T4, T5, T6, and T7 periods, respectively. The  $\text{NO}_x$  removal efficiency in the T7 period is higher than that in the T5 period because the  $\text{NaOH}$  solution in T7 contains 1.0%  $\text{Na}_2\text{SO}_3$ .

The experimental results are presented for when the injected flow rate of the  $\text{NaOH}$  solution is increased. The spray flow rate of cooling water is reduced in proportion to the increase in the  $\text{NaOH}$  solution spray flow rate, as the total flow rates of cooling water and  $\text{NaOH}$  solution must remain constant to maintain the gas temperature at the dry ESP inlet. Fig. 8 shows the time-dependent  $\text{NO}$  concentrations at the reactor inlet and outlet during the T8–T11 period (August 2020). The  $\text{NO}$  concentrations are converted based on an oxygen concentration of 15%. The average  $\text{NO}$  concentrations at the reactor inlet and outlet during the T8, T9, T10, and T11 periods are 210, 214, 204, and 210 ppm, and 217, 149, 208, and 146 ppm, respectively. During the T8 and T10 periods, the  $\text{NO}$  concentrations at the inlet and outlet of the reactor are nearly the same, indicating that  $\text{NO}$  oxidation does not occur due to other factors, such as  $\text{O}_2$ . During the T9 and T11 periods,  $\text{NO}$  at the reactor outlet is oxidized to  $\text{NO}_2$ , and the concentration of  $\text{NO}$  decreases upon the injection of  $\text{O}_3$  into the localized cooling zone formed by the three-fluid nozzles.

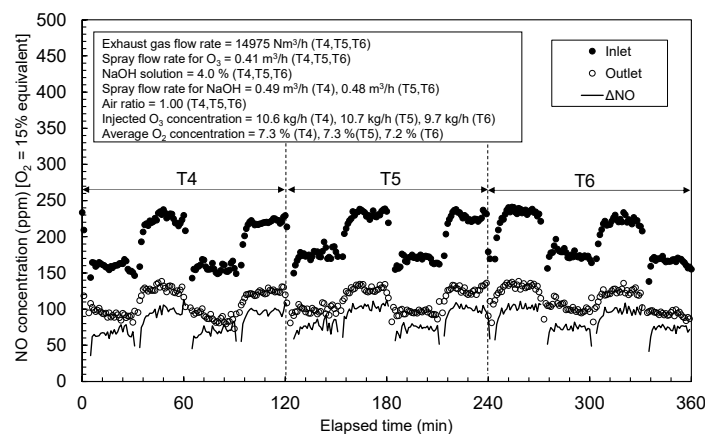


**Fig. 11.** Time-dependent  $\text{NO}$  concentrations at the reactor inlet and outlet in the T4–T6 test periods (October 2020).

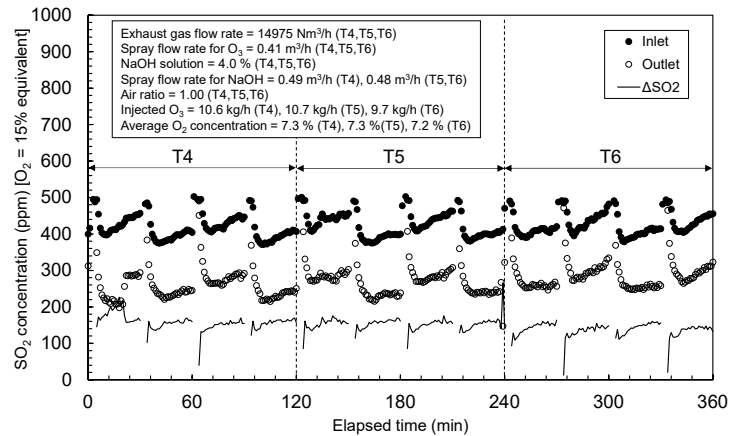


**Fig. 12.** Time-dependent  $\text{SO}_2$  concentrations at the reactor inlet and outlet in the T4–T6 test periods (October 2020).

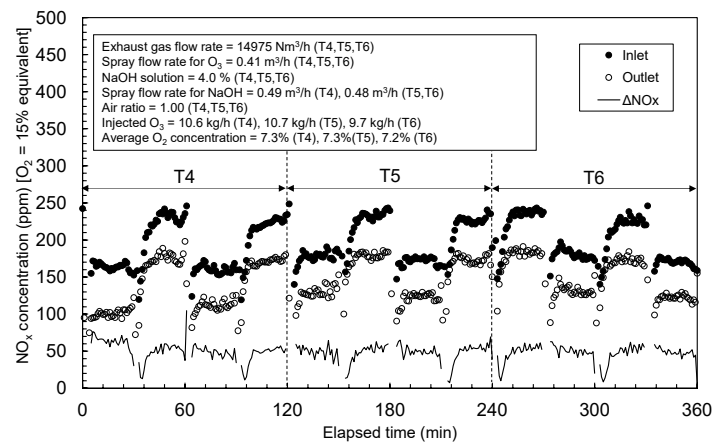


**Fig. 13.** Time-dependent  $\text{NO}_x$  concentrations at the reactor inlet and outlet in the T4–T6 test periods (October 2020).

The molar ratios of the injected  $\text{O}_3$  to  $\text{NO}$  in the exhaust gas during the T9 and T11 periods are 0.70 and 0.72, respectively. The ratio of the difference in molar flow rates of  $\text{NO}$  at the reactor inlet and outlet to the molar flow rate of the injected  $\text{O}_3$  ( $\Delta\text{NO}/\text{O}_3$ ) during the T9 and T11 periods is 0.40 in both periods, with  $\text{NO}$  removal efficiencies of 28% and 29%, respectively. The results indicate that the localized cooling zone was reduced due to the decreased flow rate of the water spray. Fig. 9 shows the time-dependent  $\text{SO}_2$  concentrations at the reactor inlet and outlet during the T8–T11 periods (August 2020). The average  $\text{SO}_2$  concentrations at the reactor inlet and outlet during the T8, T9, T10, and T11 periods are 402, 411, 425, and 405 ppm, and 286, 213, 305, and 210 ppm, respectively.  $\text{SO}_2$  removal efficiencies of 26%, 46%, 27%, and 47% are achieved in the T8, T9, T10, and T11 periods, respectively.  $\text{SO}_2$  removal efficiency improves with an increased  $\text{NaOH}$  solution flow rate to  $0.9 \text{ m}^3 \text{ h}^{-1}$ , even though the  $\text{NaOH}$  concentration was reduced by half (2.2–2.5%). Moreover, the injection of ozone into the reactor enhances desulfurization. The  $\text{NaOH}$  solution in T10 and T11 contains 1.0%  $\text{Na}_2\text{SO}_3$ ; however, the effect of  $\text{Na}_2\text{SO}_3$  on desulfurization is not observed. Fig. 10 shows the time-dependent  $\text{NO}_x$  concentrations at the reactor inlet and outlet during the T8–T11 periods (August 2020). The average  $\text{NO}_x$  concentrations at the reactor inlet and outlet during the T8, T9, T10, and T11 periods are obtained as 212, 216, 204, and 212 ppm, and 219, 169, 204, and 166 ppm, respectively.

The  $\text{NO}_x$  concentrations at the reactor inlet and outlet during the T8 and T10 periods are similar. The  $\text{NO}_x$  component is primarily  $\text{NO}$  because the concentration of  $\text{NO}_x$  does not change, meaning the denitration effect is not achieved. In the T9 and T11 periods,  $\text{NO}$  is oxidized to  $\text{NO}_2$ .  $\text{NO}_x$  removal efficiencies of 0%, 19%, 0%, and 20% are observed in the T8, T9, T10, and T11 periods, respectively. These results show that  $\text{SO}_2$  and  $\text{NO}_x$  removal efficiencies increase as the spray flow rate of the  $\text{NaOH}$  solution increases. Increasing the  $\text{NaOH}$  solution flow rate enhances  $\text{NO}_x$  removal by increasing  $\text{SO}_3^{2-}$  levels and improving the gas-liquid reaction. However, decreasing the spray flow rate of cooling water reduces  $\text{NO}$  removal efficiency, which in turn

decreases NO<sub>x</sub> removal efficiency. These opposing effects offset each other, resulting in no change in NO<sub>x</sub> removal efficiency. In the T11 period, NO<sub>x</sub> removal efficiency is the same as in the T5 period, despite the NaOH solution in T11 containing 1.0% Na<sub>2</sub>SO<sub>3</sub>. This indicates that sufficient SO<sub>3</sub><sup>2-</sup> is supplied by the SO<sub>2</sub> absorption of NaOH to react with NO<sub>2</sub>.

**Table 3.** PM concentration at reactor inlet, reactor outlet, and stack inlet.

Measurement point	PM concentration, g m <sup>-3</sup>					PM collection efficiency, %
	No. 1	No. 2	No. 3	No. 4	Average	
Reactor inlet	0.031	0.022	0.043	0.03	0.032	–
Reactor outlet	0.19	0.26	0.34	0.25	0.26	98
Stack inlet	0.002	0.007	–	–	0.005	

To balance NO and NO<sub>x</sub> removal efficiencies, the spray flow rates were maintained constant, and the nozzle tips alternated between horizontal and 30° upward orientations, depending on the nozzle position. The spray angles were set to 20° and 60°. The spray nozzles at positions 1, 3, 5, and 7 were installed at a 30° upward orientation with a 20° spray angle, while those at positions 2, 4, and 6 were installed horizontally with a 60° spray angle, as shown in Fig. 4. Fig. 11 presents the time-dependent NO concentrations at the reactor inlet and outlet during the T4–T6 periods (October 2020). The NO concentrations are normalized to an oxygen concentration of 15%. The average NO concentrations at the reactor inlet and outlet during the T4, T5, and T6 periods were 189, 199, and 197 ppm, and 107, 111, and 111 ppm, respectively. The molar ratios of injected O<sub>3</sub> to NO in the exhaust gas during these periods were 0.68, 0.72, and 0.81, respectively. The ratio of the difference in molar flow rates of NO at the reactor inlet and outlet to the molar flow rate of the injected O<sub>3</sub> ( $\Delta\text{NO}/\text{O}_3$ ) during the T4, T5, and T6 periods was 0.59, 0.62, and 0.67, with NO removal efficiencies of 41%, 44%, and 54%, respectively. Fig. 12 depicts the time-dependent SO<sub>2</sub> concentrations at the reactor inlet and outlet during the T4–T6 periods (October 2020). The average SO<sub>2</sub> concentrations at the reactor inlet and outlet during the T4, T5, and T6 periods were 419, 425, and 426 ppm, and 258, 268, and 286 ppm, respectively. Corresponding SO<sub>2</sub> removal efficiencies of 20%, 22%, and 34% were achieved during these periods. Fig. 13 illustrates the time-dependent NO<sub>x</sub> concentrations at the reactor inlet and outlet during the T4–T6 periods (October 2020). The average NO<sub>x</sub> concentrations at the reactor inlet and outlet during the T4, T5, and T6 periods were 188, 198, and 197 ppm, and 135, 147, and 148 ppm, respectively. As a result, NO<sub>x</sub> removal efficiencies of 16%, 17%, and 32% were achieved during the T4, T5, and T6 periods, respectively.

Finally, the collection of PM by the dust collectors is examined. Table 3 presents the PM concentrations at the reactor inlet, reactor outlet, and stack inlet, along with the PM collection efficiency. Measurements were conducted four times at the reactor inlet and outlet and twice at the stack inlet. The PM concentration increases at the reactor outlet due to the conversion of SO<sub>2</sub> into Na<sub>2</sub>SO<sub>3</sub> and Na<sub>2</sub>SO<sub>4</sub> particles. The results indicate that the dust collectors achieved a PM removal efficiency of 98%.

## 5. Conclusion

This study successfully applied the plasma-chemical hybrid process to an actual glass melting furnace exhaust gas treatment system, achieving simultaneous removal of PM, NO<sub>x</sub>, and SO<sub>2</sub>. To enhance NO<sub>x</sub> removal, the NaOH solution injection flow rate was increased, and Na<sub>2</sub>SO<sub>3</sub> was added to the NaOH solution. Additionally, the nozzle angle that sprayed the NaOH solution was adjusted to improve desulfurization efficiency with reduced NaOH consumption, while the injection zone was expanded. Simultaneous desulfurization and denitrification performances were evaluated. Increasing the spray flow rate of the NaOH solution facilitated NO<sub>x</sub> removal by increasing SO<sub>3</sub><sup>2-</sup> availability and enhancing gas–liquid reactions. However, a reduction in the cooling water spray flow rate led to a decrease in NO removal efficiency, which subsequently reduced overall NO<sub>x</sub> removal efficiency.

## Acknowledgment

The authors express their gratitude to Dr. H. Fujishima, a researcher at Osaka Prefecture University, for his invaluable advice on this study. Special thanks are also extended to Mr. R. Tsuji and Mr. K. Yamakawa of Nihon Yamamura Glass Co., Ltd., for their support in conducting the experiments. This study was subsidized by the Strategic Innovation Program for Energy Conservation Technologies (Project No. JPNP12004) of the New Energy and Industrial Technology Development Organization (NEDO).

## References

- [1] Zhou J., Zhou S., and Zhu Y., Experiment and prediction studies of marine exhaust gas SO<sub>2</sub> and particle removal based on NaOH solution with a U-type scrubber, *Ind. Eng. Chem. Res.*, Vol. 56 (3), pp. 12376–12384, 2017.
- [2] Li J., Chang H., Ma L., Hao J., and Yang R. T., Low-temperature selective catalytic reduction of NO<sub>x</sub> with NH<sub>3</sub> over metal oxide and zeolite catalysts—A review, *Catal. Today*, Vol. 175, pp. 147–156, 2011.
- [3] Majeed J. G., Korda B., and Békássy-Molnár E., Comparison of the efficiencies of sulfur dioxide absorption using calcium carbonate slurry and sodium hydroxide solution in an ALT reactor, *Gas Sep. Purif.*, Vol. 9 (2), pp. 111–120, 1995.
- [4] Yang B., Shen Y., Shen S., and Zhu S., Regeneration of the deactivated TiO<sub>2</sub>-ZrO<sub>2</sub>-CeO<sub>2</sub>/ATS catalyst for NH<sub>3</sub>-SCR of NO<sub>x</sub> in glass furnace, *J. Rare Earths*, Vol. 31 (2), pp. 130–136, 2013.
- [5] Hayakawa Y., Inoue Y., Takeyama A., and Kambara S., Reaction mechanism of De-NO<sub>x</sub> by activated ammonia generated by dielectric barrier discharge, *Int. J. Plasma Environ. Sci. Technol.*, Vol. 10 (1), pp. 20–23, 2016.
- [6] Noda, S., Parwatha I. G., Nada Y., Nishio S., and Fukushige S., Effect of flow field on NO<sub>x</sub> emission properties of jet nonpremixed flames in cylindrical furnaces, *J. Environ. Eng.*, Vol. 2 (4), pp. 730–739, 2007.
- [7] Uejima, M., Iwaki R., Wakimura M., Noda S., and Onuma Y., Premixing combustion of a lifted non-premixed flame in hot airstreams and NO<sub>x</sub> reduction, *Trans. Jpn. Soc. Mech. Eng. Seri. B.*, Vol. 71 (701), pp. 310–315, 2005 (in Japanese).
- [8] Okubo M., and Kuwahara T., *New Technologies for Emission Control in Marine Diesel Engines*, Elsevier, Amsterdam, The Netherlands 2019.
- [9] Kuwahara T., Yoshida K., Kuroki T., Hanamoto K., Sato K., and Okubo M., Pilot-scale combined reduction of accumulated particulate matter and NO<sub>x</sub> using nonthermal plasma for marine diesel engine, *IEEE Trans. Ind. Applicat.*, Vol. 56 (2), pp.1804–1814, 2020.
- [10] Kuwahara T., Yoshida K., Hanamoto K., Sato K., Kuroki T., and Okubo M., A pilot-scale experiment for total marine diesel emission control using ozone injection and nonthermal plasma reduction, *IEEE Trans. Ind. Appl.*, Vol. 51 (2), pp. 1168–1178, 2015.
- [11] Kuwahara T., Yoshida K., Hanamoto K., Sato K., Kuroki T., Yamamoto T., and Okubo M., Pilot-scale experiments of continuous regeneration of ceramic diesel particulate filter in marine diesel engine using nonthermal plasma-induced radicals, *IEEE Trans. Ind. Applicat.*, Vol. 48 (5), pp. 1649–1656, 2012.
- [12] Balachandran W., Manivannan N., Belega R., Abbod M. F., Brennen D., Alozie N. S. and Ganippa L. C., Nonthermal plasma system for marine diesel engine emission control, *IEEE Trans. Ind. Applicat.*, Vol. 52 (3), pp. 2496–2505, 2016.
- [13] Fujishima H., Tatsumi A., Kuroki T., Tanaka A., Otsuka K., Yamamoto T., and Okubo M., Improvement in NO<sub>x</sub> removal performance of the pilot-scale boiler emission control system using an indirect plasma–chemical process, *IEEE Trans. Ind. Applicat.*, Vol. 46 (5), pp. 1722–1729, 2010.
- [14] Chang J. S., Urashima K., Tong Y. X., Liu W. P., Wei H. Y., Yang F. M., and Liu X. J., Simultaneous removal of NO<sub>x</sub> and SO<sub>2</sub> from coal boiler flue gases by DC corona discharge ammonia radical shower systems: pilot plant tests, *J. Electrostat.*, Vol. 57 (3), pp. 313–323, 2003.
- [15] Li S., Huang Y., Wang F., Liu J., Feng F., Shen X., Zheng Q., Liu Z., Wang L., and Yan K., Fundamentals and environmental applications of non-thermal plasmas: multi-pollutants emission control from coal-fired flue gas, *Plasma Chem. Plasma Process.*, Vol. 34, pp. 579–603, 2014.
- [16] Mok Y. S., and Lee H. J., Removal of sulfur dioxide and nitrogen oxides by using ozone injection and absorption–reduction technique, *Fuel Process. Technol.*, Vol. 87 (7), pp. 591–597, 2006.
- [17] Lee Y. H., Jung W. S., Choi Y. R., Oh J. S., Jang S. D., Son Y. G., Cho M. H., Namkung W., Koh D. J., Mok Y. S., and Chung J. W., Application of pulsed corona induced plasma chemical process to an industrial incinerator, *Environ. Sci. Technol.*, Vol. 37 (11), pp. 2563–2567, 2003.
- [18] Chang M. B., Lee H. M., Wu F., and Lai C. R., Simultaneous removal of nitrogen oxide/nitrogen dioxide/sulfur dioxide from gas streams by combined plasma scrubbing technology, *J. Air Waste Manage. Assoc.*, Vol. 54 (8), pp. 941–949, 2004.

- [19] Kim H. J., Han B., Woo C. G., and Kim Y. J., NO<sub>x</sub> removal performance of a wet reduction scrubber combined with oxidation by an indirect DBD plasma for semiconductor manufacturing industries, *IEEE Trans. Ind. Applicat.*, Vol. 54 (6), pp. 6401–6407, 2018.
- [20] Zhou J., Zhou S., and Zhu Y., Experiment and prediction studies of marine exhaust gas SO<sub>2</sub> and particle removal based on NaOH solution with a U-type scrubber, *Ind. Eng. Chem. Res.*, Vol. 56 (43), pp. 12376–12384, 2017.
- [21] T. Kuroki T., Yamamoto H., Fujishima H., Takada D., Yamato Y., and Okubo M., NO<sub>x</sub> removal for flue gas in glass furnace using an ozone injection chemical hybrid process – laboratory experiments with semi-dry model system, *J. Inst. Electrostat. Jpn.*, Vol. 38 (1), pp. 52–58, 2014. (in Japanese)
- [22] Yamamoto Y., Yamamoto H., Takada D., Kuroki T., Fujishima H., and Okubo M., Simultaneous removal of NO<sub>x</sub> and SO<sub>x</sub> from flue gas of a glass melting furnace using a combined ozone injection and semi-dry chemical process, *Ozone: Sci. Eng.*, Vol. 38 (3), pp. 211–218, 2016.
- [23] Yamasaki H., Mizuguchi Y., Maeda K., Fujishima H., Kuroki T., Yamamoto H., and Okubo M., Performance evaluation of semi-dry flue gas desulfurization and denitration from flue gas of a glass melt using nonthermal plasma combined process, *Mech. Eng. J.*, Vol. 8 (2), 20-00519, 2021.
- [24] Yamasaki H., and Koizumi Y., Numerical simulation of semi-dry flue gas denitration using water-cooled ozone injection method, *Int. J. Plasma Environ. Sci. Technol.*, Vol. 15 (2), e02011, 2021.
- [25] Yamamoto H., Kuroki T., Fujishima H., and Okubo M., Pilot-scale exhaust gas treatment for a glass manufacturing system using a plasma combined wet chemical process, *Mech. Eng. J.*, Vol. 3 (1), 15-00549, 2016.
- [26] Yamamoto H., Kuroki T., Fujishima H. and Okubo M., Pilot-scale NO<sub>x</sub> and SO<sub>x</sub> aftertreatment using a two-phase ozone and chemical injection in glass-melting-furnace exhaust gas, *IEEE Trans. Ind. Applicat.*, Vol. 55 (6), pp. 6295–6302, 2019.
- [27] Yamasaki H., Mizuguchi Y., Nishioka R., Fukuda Y., Kuroki T., Yamamoto H., and Okubo M., Pilot-scale NO<sub>x</sub> and SO<sub>x</sub> aftertreatment by semi-dry plasma-chemical hybrid process in glass-melting-furnace exhaust gas, *Plasma Chem. Plasma Process.*, Vol. 42, pp. 51–71, 2021.
- [28] Yamasaki H., Nishioka R., Fukuda Y., Kuroki T., Yamamoto H., and Okubo M., Energy-saving glass-melting-furnace with semi-dry plasma-chemical hybrid process, *Plasma Process. Polym.*, Vol. 21, e2300078, 2024.